LAWRENCE
LIVERMORE
NATIONAL
LABORATORY

LLNL-PROC-759466

Thermal Safety Modeling of TATB-based Explosive

Jason S. Moore, Matthew A. McClelland, Peter C. Hsu, German F. Ellsworth, Evan M. Kahl, and Harry K. Springer

July 2018

16th International Detonation Symposium
Cambridge, MD, July 15-20, 2018

Thermal Safety Modeling of TATB-based Explosive

Jason S Moore, Matthew A. McClelland, Peter C. Hsu, German F. Ellsworth, Evan M. Kahl, and Harry K. Springer

Lawrence Livermore National Laboratory, Livermore, CA 94551

Abstract. We investigate and model the cook-off behavior of TATB-based (2,4,6-triamino-1,3,5-trinitrobenzene) high explosives (HE) because this knowledge is critical to understanding system response in abnormal thermal environments. Thermal decomposition of TATB has been explored in conventional ODTX (One-Dimensional Time-to-eXplosion), PODTX (ODTX with Pressure-measurement), TGA (thermogravimetric analysis), and DSC (differential scanning calorimetry) experiments under isothermal and multiple ramped temperature profiles.

These experimental data have been used together to fit reaction rate parameters for proposed reaction schemes in LLNL's multi-physics hydrocode, ALE3D (Arbitrary Lagrangian-Eulerian 3D and 2D). This model includes chemical reactions, thermo- and hydro-dynamics, and material properties, including thermal expansion, compressibility, and strength. We employ a Python evolutionary algorithm to optimize reaction rate parameters on high performance computing clusters. Once experimentally validated, this model will be scalable to several applications involving TATB-based HEs and can be used to develop more sophisticated experimental methods. Furthermore, the modeling and optimization methodology developed herein should be applicable to other high explosive materials.

Introduction

Understanding the thermal response of high explosives (HE) is central to predicting response during and after accident scenarios. One energetic material currently being employed extensively in industrial and military applications is 1,3,5-triamino-2,4,6-trinitrobenzene (TATB), due to its high thermal stability and low shock sensitivity. However, much is still left to be understood about its thermal decomposition pathways, including conflicting conclusions as to the effect of confinement[1] and whether the dominant decomposition mechanism includes gas-phase species.

Recent work by Hobbs and Kaneshige[1] included the effect of the initial water content, which can be on the order of hundreds to thousands of ppm.[2] Including the water vapor-liquid equilibrium greatly improves the accuracy of modeled pressure during early decomposition. Additionally, several studies have shown that the decomposition of TATB yields a large quantity of water; experimental[3,4] and computational[5] studies indicate that the likely first step in decomposition is a condensation reaction to form monobenzofurazan. However, disagreement still exists as to whether this and subsequent reactions are primarily intra- or inter-molecular. Additionally, TATB may react, probably inter-molecularly, to form monobenzo-furoxan (Fig. 1).

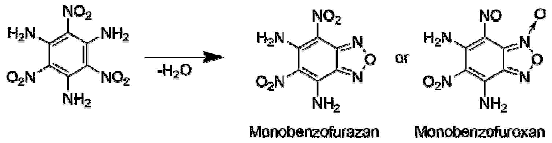

Fig. 1. Initial TATB condensation reactions.

Moreover, little is known about what happens between these initial reactions and final thermal runaway. Experiments have shown that the monobenzo-furazan and -furoxan can continue to dehydrate to form di- and tri-benzo species. The model discussed herein focuses on the most reduced, likely form of the reaction network, excluding the furoxan species and later dehydration intermediates, which may not be along pathways necessary to reach final decomposition products. Our reaction scheme is shown in Fig. 2, wherein TATB dehydrates intramolecularly, the mono-intermediates (MF) decompose inter-molecularly into gas and solid products, and the gas products further autocatalyze decomposition of TATB. Furthermore, the hydro-code enables the gas products to be modeled as a gas phase concentration utilizing appropriate material properties, expansion, and compressibility dependent upon local spatial conditions, rather than as a mixed phase species. While the product gas has been observed to contain several species,[3] the kinetics utilized mass rather than mole concentrations, meaning specific product molecular weights and compositions did not have to be assumed. This scheme was chosen based on the ability to fit experimental data with consideration of initial results from forthcoming experiments,[6-10] while requiring a minimal number of fitted parameters. Moreover, this scheme provides appropriate density dependence for Time-To-eXplosion (TTX) and would account for experimentally observed lower TTX in ultrafine TATB as compared to course TATB of the same density due to increased specific surface area.[11]

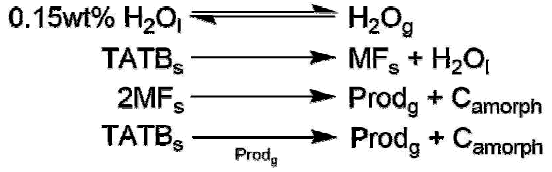

Fig. 2. TATB decomposition scheme.

Fig. 3a shows the main experimental apparatus used here to examine cookoff behavior is the One Dimensional Time to eXplosion (ODTX), which has recently been augmented with Pressure measurements (PODTX).[12] Fig. 4 shows typical temperature profiles used in these experiments. Half-inch diameter spheres of HE are either delivered to preheated anvils, which are rapidly closed for isothermal ODTX experiments or subjected to controlled temperature ramps, possibly with isothermal holds, for PODTX experiments. PODTX experiments were not done with initially heated anvils due to concerns the rapid closing might cause damage to pressure transducers. This system can also be used to thermally damage samples to examine chemical and behavior changes without continuing to thermal runaway (Fig. 3b).

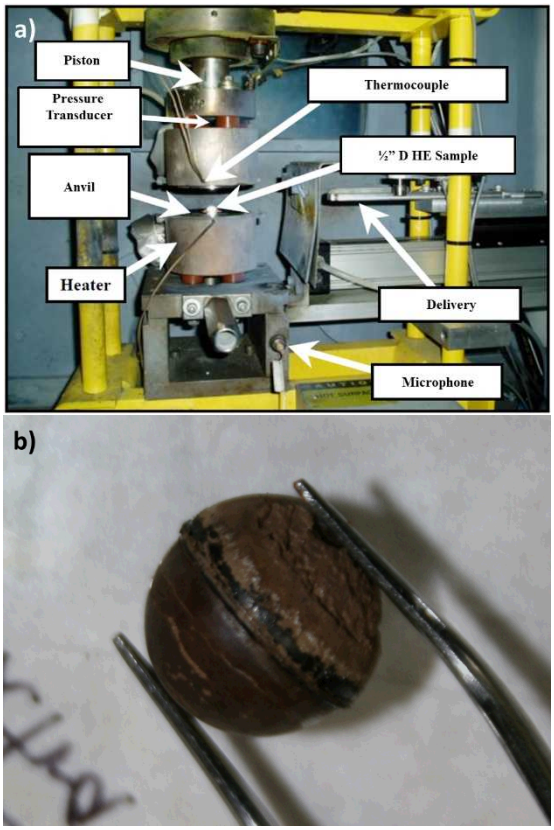

Fig. 3. a) (P)ODTX experimental setup with b) thermally cycled spherical HE sample.

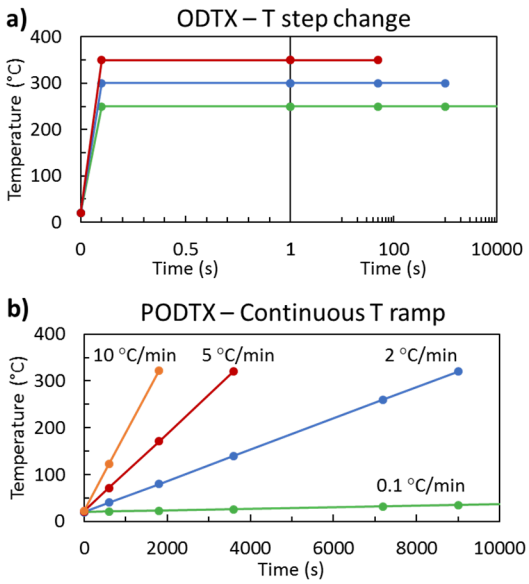

Fig. 4. a) ODTX and b) PODTX example temperature curves.

(P)ODTX time to explosion or pressure burst, thermo-gravimetric analysis (TGA), and differential scanning calorimetry (DSC) experiments were simulated using ALE3D[13] and compared to experimental results. This model includes chemical reactions, thermo- and hydro-dynamics, and material properties (see Table 1), including thermal expansion, compressibility, and strength.[14] The activation energy, E_A, and an orthogonalized pre-exponential factor, k_0, for each of the three decomposition reactions, j, in Fig. 2, giving reaction rates

$$k_j = k_{0,j} \exp\left[-E_{A,j}\left(\frac{1}{T} - \frac{1}{T_0}\right)\right] \quad (1)$$

were varied using the Python[15] SciPy[16] differential evolution algorithm,[17] which was modified to update only after completing a generation rather than as each calculation finished to allow for parallelization and flexibility in use of computational resources.

The objective function

$$\min \sum_{i=1}^{Nexp} \left(ln\left({}^{t_{sim,i}}/_{t_{exp,i}} \right) \right)^2 \quad (2)$$

was minimized, where $t_{sim,i}$ and $t_{exp,i}$ are the simulated and experimental times, respectively, for the ith experiment. For (P)ODTX experiments, the simulated endpoint was determined when either the calculation time step dropped below 1 μs, indicating thermal runaway due to rapid chemical reaction, or the pressure at the boundary between the HE and anvils reached the burst pressure of 1500 or 2000 bar, depending on the exact experimental apparatus used. To prevent anomalously predicting pressure bursts at higher temperatures, simulations for ODTX experiments above 280 °C were only allowed to terminate by thermal runaway.[11] For DSC, the full-width half max of the exothermic peak was compared. For TGA, the times at 0.5, 5, and 50% mass loss were compared.

Results

Time-to-explosion due to thermal runaway or pressure burst simulation and experiment results for LX-17 (92.5% TATB, 7.5% Kel-F) at several ranges of theoretical maximum density (TMD) are compared in Fig. 5.

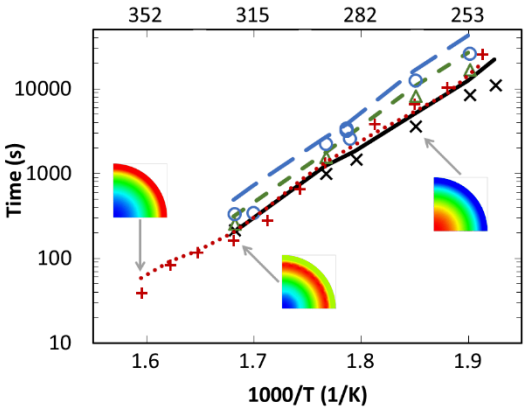

Fig. 5. LX-17 ODTX explosion/burst time for 98-100% TMD experiment (×) and model (black line), 94-97% TMD experiment (+) and model (red dotted line), 92-93% TMD experiment (Δ) and model (green short-dashed line), and 85-89% TMD experiment (○) and model (blue long-dashed line).

Experimental and model results show a trend of increasing time to explosion as TMD decreases. The inset pictures show the simulated temperature profiles for some of the ODTX ALE3D runs. Fig. 6 shows the general simulation layout, where the HE was simulated as a quarter circle with axial and radial symmetry with a surrounding aluminum

shell, where the temperature boundary condition (BC) was applied as per Fig. 4. At lower temperatures, the experiment begins to self-heat at the center due to exothermic decomposition. In contrast, at higher temperatures, the heat does not have time to fully conduct into the HE spheres before significant decomposition occurs at or near the outer edge of the HE. Similar results for PBX-9502 (95% TATB, 5% Kel-F), which were not used for model fitting, are shown in Fig. 7.

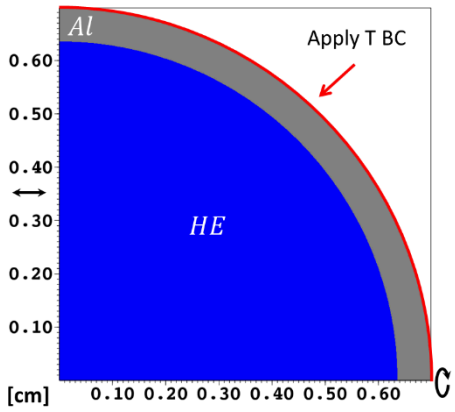

Fig. 6. ALE3D (P)ODTX model diagram.

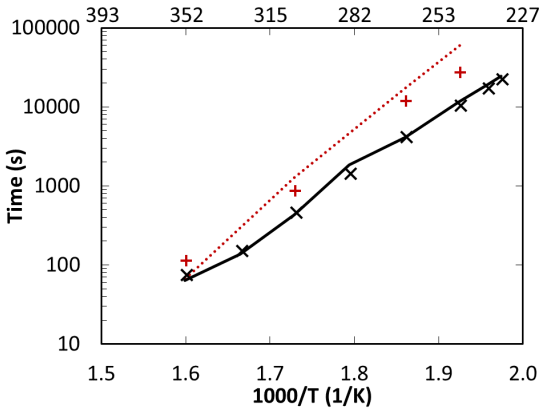

Fig. 7. PBX-9502 ODTX explosion/burst time for 98% TMD experiment (×) and model (black line) and 85% TMD experiment (+) and model (red dotted line).

A modified version of the numerical mesh was employed for the PODTX simulations, due to modifications to the experimental setup and use of a temperature ramp. The aluminum anvils were replaced with stainless steel, and the full 3" diameter was modeled to capture temperature gradients in the anvil. At the lower ramp rates, the experiment is expected to be largely isothermal throughout, while at higher ramp rates, a significant temperature gradient exists between the temperature controller at the steel exterior and the center of the HE.

The PODTX model and experimental results are shown in Fig. 8 for 86% and 98% TMD LX-17 at multiple ramp rates from 0.1 to 8 °C/min. The model predicts similar trends in time to explosion as the experiment; however, some offset is seen at present.

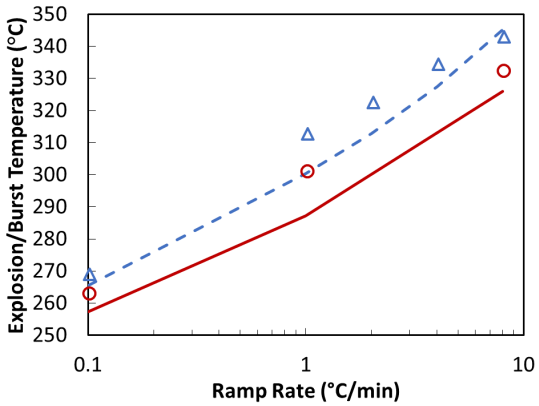

Fig. 8. LX-17 PODTX explosion/burst time for 98% TMD experiment (○) and model (red line) and 86% TMD experiment (Δ) and model (blue dashed line).

The pressures at 98% and 86% TMD and 1 °C/min are shown in Fig. 9 for the experiment and model. During the anvil redesign between ODTX and PODTX experiments, the inner cavity diameter was slightly increased from 0.25 to 0.265 inches, but the same size HE sphere is used. To accommodate this difference, a metal sleeve is used in the lower anvil to bridge the additional volume. However, experiments are run with an air gap between the upper HE surface and anvil to facilitate pressure equilibrium for sensing. Thus, initially there is approximately 10% free volume into which the HE expands as it is heated, leading to the hemispherical differences seen in Fig. 3b. This excess volume is accounted for in the pressure calculation; however, as the model does not

presently include porous flow, no gas products or evaporated water leave the HE material.

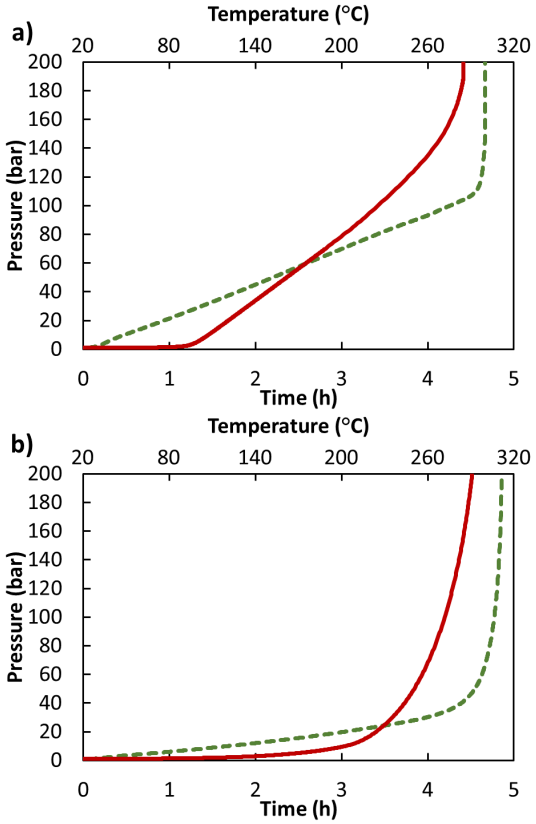

Fig. 9. PODTX pressure in 1 °C/min experiment (green dashed line) and model (red line) for a) 98% TMD and b) 86% TMD.

Lastly, simultaneous thermo-gravimetric analysis (TGA) and differential scanning calorimetry (DSC) measurements were run with small (5-10 mg) samples of TATB in a pinhole pan at 1 °C/min. Mass loss and heat flow results and model calculations are shown in Fig. 10. The model was fit using three points along the TGA curve (0.5, 5, and 50% mass loss) and the full-width half max (FWHM) of the DSC curve.

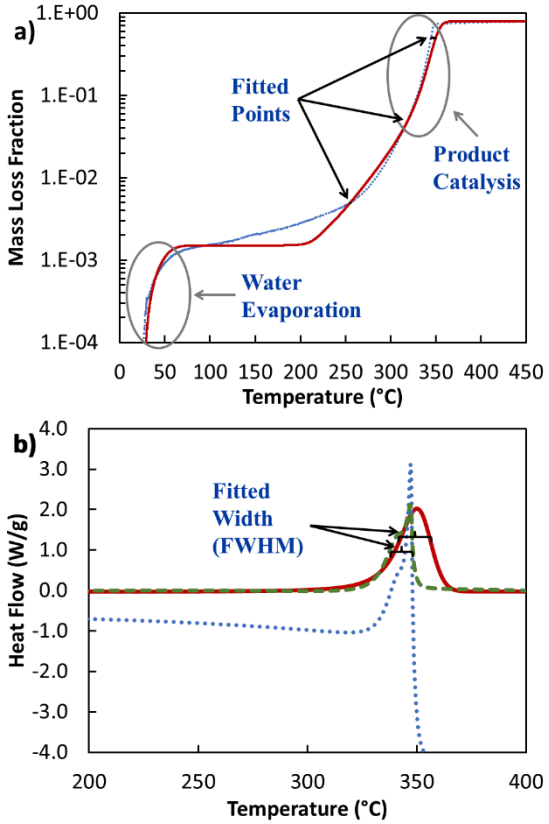

Fig. 10. TATB experiment (blue dotted line) and model (red line) for a) TGA and b) DSC. Heat flow after endotherm baseline shift (green dashed line).

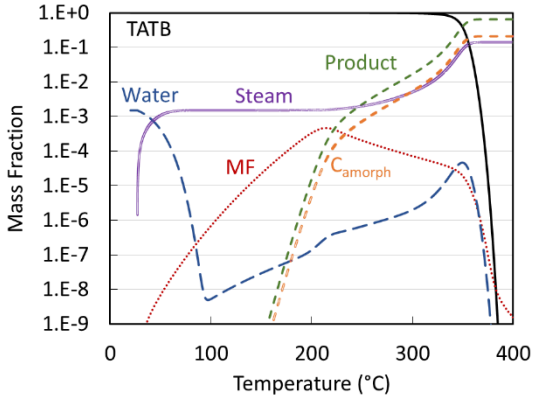

Fig. 11. Modeled species concentrations in TGA/DSC: TATBa (black line), TATBb (red dotted line), TATBc (green short-dashed line), water (blue long-dashed line), steam (purple double

line), and amorphous carbon (orange double dashed line).

Both PODTX and TGA results indicate that some lower temperature reaction is not entirely accounted for in the model. In the TGA, this effect may largely be due to sublimation, which is not in the model. While a pinhole pan significantly reduces the amount of sublimation as compared to an open pan, the raw heat flow still shows a significant endotherm. As the (P)ODTX system is sealed, little sublimation is expected to occur. Thus, for purposes of comparing to the model, the DSC data was shifted to remove the endotherm. With the level of confinement used in the (P)ODTX systems, the early gas formation does not appear to have a significant impact on TTX; however, in lower confinement systems, this may not be the case.

Conclusions

LX-17 cookoff was modeled with ALE3D and compared to several experiments. Time-to-explosion was well predicted under isothermal and ramped heating conditions. Work is currently ongoing to measure chemical composition of reaction products in both solid and gas phase during experiments, as well as analysis of solid residue in aged and spent materials. These results should significantly inform model development, especially related to intermediate species, which until now has largely relied only upon time-to-explosion endpoint data.

Audience Questions

1. Did you use pressure explicitly to modify your rates? Do you model vented systems? If so, do you model gas transport and material damage?

Gas-phase concentrations are calculated depending upon pressure. Vented systems and pore transport are not presently accounted for in the model.

2. On the figure that shows monofurazan, water carbon, TATB, etc., were these concentrations determined experimentally?

These are modeled concentrations. Reaction intermediates are currently being synthesized to use as standards to accurately determine final experimental compositions.

Table 1. Model nomenclature and physical properties.

Material	Symbol	Description	Value	Units
LX-17	C_v	Constant volume heat capacity[18]	1.13	J/g·K
	k_{293}	Thermal conductivity at 293 K[18]	0.799	W/m·K
	ρ	Theoretical maximum density[18]	1.94	g/cm^3
	G_0	Initial shear modulus[14]	6.62E-02	Mbar
	Y_0	Initial yield strength[14]	2.05E-04	Mbar
	A_0	$1/\left(G_0(dG/dP)\right)$[14]	0	1/Mbar
	B_0	$1/\left(G_0(dG/dT)\right)$[14]	5.46E-02	1/K
	P	$0.0408\mu + 1.137\mu^2 - 0.183\mu^3 + (0.491 + 0.491\mu)E$		Mbar
	μ	$V_0/V - 1$		--
TATBa [a]	k_{293}	Thermal conductivity at 293 K[19]	0.879	W/m·K
	k_{673}	Thermal conductivity at 673 K[19]	0.418	W/m·K
	ΔH_f^{298}	Heat of formation at 298 K[20]	-542.4	J/g
TATBb [a]	ΔH_f^{298}	Heat of formation at 298 K [b]	596.2	J/g
TATBc [c]	ΔH_f^{298}	Heat of formation at 298 K [d]	-1782.2	J/g
Kel-F [a]	k_{273}	Thermal conductivity at 273 K[21]	0.053	W/m·K
	ρ	Reference density[22]	2.12	g/cm^3
	ΔH_f^{298}	Heat of formation at 298 K [e]	0	J/g
Water	C_v	Constant volume heat capacity[23]	4.138	J/g·K
	k_{273}	Thermal conductivity at 273 K[23]	0.561	W/m·K
	k_{373}	Thermal conductivity at 373 K[23]	0.679	W/m·K
	k_{673}	Thermal conductivity at 673 K[23]	0.695	W/m·K
	ΔH_f^{298}	Heat of formation at 298 K[23]	-15860	J/g
	ρ	Reference density[23]	0.997	g/cm^3
Steam	C_v	Constant volume heat capacity[23]	1.5558	J/g·K
	k_{373}	Thermal conductivity at 373 K[23]	0.0251	W/m·K
	k_{673}	Thermal conductivity at 673 K[23]	0.0548	W/m·K
	k_{1273}	Thermal conductivity at 1273 K[23]	0.1363	W/m·K
	γ	Heat capacity ratio[23]	1.337	--
	ΔH_f^{298}	Heat of formation at 298 K[23]	-13556	J/g
	ρ	Reference density[23]	6.40E-04	g/cm^3
C_{amorph}	C_v	Constant volume heat capacity[24]	0.43	J/g·K
	k_{273}	Thermal conductivity at 273 K[24]	1.508	W/m·K
	k_{673}	Thermal conductivity at 673 K[24]	2.235	W/m·K
	k_{1273}	Thermal conductivity at 1273 K[24]	3.000	W/m·K
	ΔH_f^{298}	Heat of formation[23]	0	J/g
	ρ	Reference density[20]	2.1	g/cm^3
Air [f]	C_v	Constant volume heat capacity[5]	0.743	J/g·K
	k_{273}	Thermal conductivity at 273 K[5]	0.0254	W/m·K

[a] Use LX-17 properties unless otherwise specified.
[b] Set so ΔH_r: TATBa → TATBb + H_2O(g) = 39 kJ/mol [10]
[c] Use N_2 properties unless otherwise specified.
[d] Set so ΔH_r: TATBa → TATBc + 2H_2O(g) + 4.5 C_{amorph} = 2500 kJ/mol [4]
[e] Modeled as inert.
[f] Use N_2 properties.

	k_{673}	Thermal conductivity at 673 K[5]	0.0481	W/m·K
	k_{1273}	Thermal conductivity at 1273 K[5]	0.0797	W/m·K
	γ	Heat capacity ratio[5]	1.401	--
	ρ	Reference density[5]	1.17E-03	g/cm^3

Acknowledgements

This work was performed under the auspices of the U.S. DOE by LLNL under contract DE-AC52-07NA27344. LLNS, LLC.

The authors wish to thank Ben Yancey and Jennifer Montgomery for DSC and TGA data, Steve Strout for P/ODTX runs, and John Reynolds for sensitization analysis.

References

[1] M. L. Hobbs and M. J. Kaneshige, "Ignition Experiments and Models of a Plastic Bonded Explosive (PBX 9502)," *The Journal of Chemical Physics,* vol. 140, 2014.

[2] W. S. IV, E. A. Glascoe and G. E. Overturf, "Measurement of Moisture Outgassing of the Plastic-Bonded TATB Explosive LX-17," *Thermochimica Acta,* vol. 545, pp. 90-95, 2012.

[3] T. A. Land, W. J. Siekhaus and M. F. Foltz, "Condensed-Phase Thermal Decomposition of TATB Investigated by Atomic Force (AFM) and Simultaneous Thermogravimetric Modulated Beam Mass Spectrometry (STMBMS)," in *International Detonation Symposium*, Boston, 1993.

[4] J. Sharma, J. W. Forbes, C. S. Coffey and T. P. Liddiard, "The Physical and Chemical Nature of Sensitization Centers Left from Hot Spots Cause in Triaminotrinitrobenzene by Shock or Impact," *Journal of Physical Chemistry,* vol. 91, pp. 5139-5144, 1987.

[5] C. J. Wu and L. E. Fried, "Ring Closure Mediated by Intramolecular Hydrogen Transfer in the Decomposition of a Push-Pull Nitroaromatic :TATB," *Journal of Physical Chemistry A,* vol. 104, pp. 6447-6452, 2000.

[6] J. M. Densmore, E. M. Kahl, E. A. Glascoe, M. A. McClelland, M. R. DeHaven, M. A. Suda and N. Tan, "Thermal Explosions of LX-17," in *International Detonation Symposium*, Cambridge, MD, 2018.

[7] P. C. Hsu, S. A. Strout, J. G. Reynolds, E. M. Kahl, A. Hye, J. S. Moore, M. A. McClelland, M. Gresshoff, G. F. Ellsworth and T. Healy, "Thermal Safety Characterization of Energetic Materials in the ODTX/P-ODTX System," in *International Detonation Symposium*, Cambridge, MD, 2018.

[8] E. M. Kahl, G. F. Ellsworth, M. R. DeHaven, M. A. Suda, P. C. Hsu, S. A. Strout, M. A. McClelland, R. A. Ryckman, J. S. Moore, K. S. Vandersall and J. G. Reynolds, "Fast & Slow Cook-off Experiments of LX-17 using Induction & Resistance Heating," in *International Detonation Symposium*, Cambridge, MD, 2018.

[9] E. M. Kahl, P. C. Hsu, K. R. Coffee, B. J. Yancey, G. F. Ellsworth, T. E. Healy and J. G. Reynolds, "Safety Assessments of Thermally Damaged Energetic Materials," in *International Detonation Symposium*, Cambridge, MD, 2018.

[10] B. J. Yancey, N. K. Muetterties, E. M. Kahl, E. A. Glascoe and J. G. Reynolds, "Evolved Gas Analysis of the THermal Decomposition of TATB and TATB-Based Plastic Bonded Explosives from the Small to Large Scales," in *International Detonation Symposium*, Cambridge, MD, 2018.

[11] C. M. Tarver and J. G. Koerner, "Effects of Endothermic Binders on Times to Explosion of HMX- and TATB-Based Plastic Bonded Explosives," *Journal of Energetic Materials,* vol. 26, pp. 1-28, 2008.

[12] P. C. Hsu, M. Howard and J. L. Maienschein, "The ODTX System for Thermal Ignition and Thermal Safety Study of Energetic Materials," in *International Detonation Symposium*, Coeur D'Alene, ID, 2010.

[13] C. Noble, A. Anderson, N. Barton, J. Bramwell, A. Capps, M. Chang, J. Chou, D. Dawson, E. Diana, T. Dunn, D. Faux, A. Fisher, P. Greene, I. Heinz, Y. Kanarska, S. Khairallah, B. Liu, J. Margraf, A. Nichols III, R. Nourgaliev, M. Puso, J. Reus, P. Robinson, A. Shestakov, J. Solberg, D. Taller, P. Tsuji, C. White and J. White, "ALE3D: An Arbitrary Lagrangian-Eulerian Multi-Physics Code," LLNL-TR-732040, Lawrence Livermore National Laboratory, 2017.

[14] M. A. McClelland, R. A. Ryckman, J. S. Moore, E. M. Kahl, J. M. Densmore, P. C. Hsu, M. R. DeHaven and G. F. Ellsworth, "ALE3D Simulation of Thermal Decomposition and Violence in Slow Cookoff Experiments with LX-17, a TATB-based Explosive," in *International Detonation Symposium*, Cambridge, MD, 2018.

[15] Python Software Foundation, "Python 2.7," https://docs.python.org/2.7/, 2018.

[16] E. Jones, T. Oliphant and P. Peterson, "SciPy: Open source scientific tools for Python," 2001. [Online]. Available: http://www.scipy.org/. [Accessed 2017].

[17] R. Storn and K. Price, "Differential Evolution - a Simple and Efficient Heuristic for Global Optimization over Continuous Spaces," *Journal of Global Optimization,* vol. 11, pp. 341-359, 1997.

[18] B. M. Dobratz, "LLNL Explosives Handbook," *Lawrence Livermore National Lab Report UCRL-52997-Chg.2,* 1985.

[19] C. M. Tarver, S. K. Chidester and A. L. Nichols, "Critical Conditions of Impact- and Shock-Induced Hot Spots in Solid Explosives," *Journal of Physical Chemistry,* vol. 100, pp. 5794-5799, 1996.

[20] Cheetah 8.0, Energetic Materials Center, *Lawrence Livermore National Lab.,* 2015.

[21] A. K. Burnham and R. K. Weese, "Kinetics of Thermal Degradation of Explosive Binders Viton A, Estane, and Kel-F," *Thermochimica Acta,* vol. 426, pp. 85-92, 2005.

[22] C. L. Choy, F. C. Chen and W. H. Luk, "Thermal Conductivity of Oriented Crystalline Polymers," *Journal of Polymer Science,* vol. 18, pp. 1187-1207, 1980.

[23] "NIST Chemistry Webbook," National Institute of Standards and Technology, 2017. [Online]. Available: https://webbook.nist.gov/chemistry. [Accessed 2017].

[24] C. L. Yaws, "Yaws' Critical Property Data for Chemical Engineers and Chemists," 2014. [Online]. Available: https://app.knovel.com/web/. [Accessed 2017].

Disclaimer